NETWORKS AND HETEROGENEOUS MEDIA
©American Institute of Mathematical Sciences
Volume **5**, Number **3**, September **2010**
doi:10.3934/nhm.2010.5.661
pp. **661–674**

THE COMPUTATION OF NONCLASSICAL SHOCK WAVES WITH A HETEROGENEOUS MULTISCALE METHOD

Frederike Kissling and Christian Rohde

Institut für Angewandte Analysis und Numerische Simulation
Universität Stuttgart
Pfaffenwaldring 57, D-70569 Stuttgart, Germany

Abstract. We consider weak solutions of hyperbolic conservation laws as singular limits of solutions for associated complex regularized problems. We are interested in situations such that undercompressive (Non-Laxian) shock waves occur in the limit. In this setting one can view the conservation law as a macroscale formulation while the regularization can be understood as the microscale model.

With this point of view it appears natural to solve the macroscale model by a heterogeneous multiscale approach in the sense of E&Engquist[7]. We introduce a new mass-conserving numerical method based on this concept and test it on scalar model problems. This includes applications from phase transition theory as well as from two-phase flow in porous media.

1. **Introduction.** We consider weak solutions of the initial-value problem

$$U_t + f(U)_x = 0 \quad \text{in} \quad \Omega_T := \mathbb{R} \times (0,T), \tag{1}$$

$$U(.,0) = U_0 \quad \text{in} \quad \mathbb{R} \tag{2}$$

for the scalar unknown $U : \mathbb{R} \times (0,T) \to \mathcal{U} \subseteq \mathbb{R}$. Hereby $U_0 : \mathbb{R} \to \mathcal{U}$ stands for the initial datum and $f \in C^3(\mathcal{U})$ is a nonlinear flux function: we assume that f'' vanishes only in finitely many points. The problem will be called the **macroscale problem** in what follows.

It is well-known that solutions of (1), (2) can have discontinuous shock wave solutions independently of the regularity of U_0. These solutions are not uniquely determined. For fluxes with $f'' \neq 0$ uniqueness can be enforced if only shock waves that satisfy the Lax condition are allowed. For the case of a discontinuous wave

$$U(x,t) = U^- \text{ for } x - st < 0 \quad \text{and} \quad U(x,t) = U^+ \text{ for } x - st > 0, \tag{3}$$

with states $U^-, U^+ \in \mathcal{U}$, $U^- \neq U^+$, and shock speed

$$s = s(U^-, U^+) = (f(U^+) - f(U^-))/(U^+ - U^-), \tag{4}$$

the Lax condition reads as

$$f'(U^+) < s < f'(U^-). \tag{5}$$

2000 *Mathematics Subject Classification.* Primary: 35L65.

Key words and phrases. Heterogeneous multiscale method, conservation laws, shock wave, nonclassical shock, phase transition, two-phase flow.

Authors are members of the International Research Training Group NUPUS, funded by the German Research Foundation (DFG) and The Netherlands Organisation for Scientific Research (NWO), and thank the DFG (GRK 1398) and NWO (DN 81-754) for their support. Also the authors would like to thank the Cluster of Excellence SimTech (EXC 310/1).

Equivalently uniqueness is ensured if the entropy inequality

$$\eta(U)_t + q(U)_x \leq 0 \tag{6}$$

holds in the weak sense for at least one entropy pair $(\eta, q) \in (C^2(\mathcal{U}))^2$, i.e. functions with $\eta'' > 0$ and q satisfying $q' = \eta' f'$.

If the flux f has at least one inflection point one can construct discontinuous waves U that violate exactly one of the conditions in (5) (with $>$ instead of $<$) but still satisfy (6) for one entropy pair. Such waves connect states such that f'' changes sign and are called undercompressive or **nonclassical**. There are various applications where they have a crucial physical importance as phase boundaries, detonation waves, infiltration fronts, or thin-film precursors. Unique solvability of the initial value problem (1), (2) can again be guaranteed if only nonclassical waves are allowed that satisfy an additional algebraic condition of type

$$\varphi(U^-, U^+) = 0, \tag{7}$$

where the given function $\varphi : \mathcal{U}^2 \to \mathbb{R}$ is called kinetic function. A wellposedness theory based on kinetic functions has been developed by LeFloch ([16] and references therein). Numerical schemes for nonclassical solutions of (1), (2) controlled by kinetic functions have just recently been developed (e.g. in [5, 3]).

In many cases an explicit kinetic relation that determines the physically relevant solution is either not known or cannot be written in closed algebraic form as in (7). Alternatively one can obtain these solutions as the singular limit

$$U^\lambda := \lim_{\varepsilon \to 0} u^{\varepsilon,\lambda} \tag{8}$$

of (unique) solutions to a family of associated regularized problem (referred to as the **microscale** model)

$$u_t^{\varepsilon,\lambda} + f(u^{\varepsilon,\lambda})_x = R^\varepsilon[\lambda; u^{\varepsilon,\lambda}] \qquad (\varepsilon > 0). \tag{9}$$

Here $R^\varepsilon[\lambda; \cdot]$ stands for a higher-order integro-differential operator which satisfies $R^0[\lambda; \cdot] \equiv 0$ (formally). It is assumed to depend on some parameter λ from a subset of $\mathbb{R}$. For many applications operators $R^\varepsilon[\lambda; \cdot]$ have been suggested and it has been proven that the limit U^λ in (8) exists (at least for some subsequences) and contains nonclassical waves. We will discuss various examples in Sect. 2.

While the regularization approach is natural from the modelling viewpoint direct numerics for (9) with fixed $0 < \varepsilon \ll 1$ is computationally expensive: shock wave layers (scaling with ε) have to be resolved and in general time steps become extremely small. Therefore we propose here a new **Heterogeneous Multiscale Method (HMM)** in the sense of E&Engquist ([7] or [19] for a related application for combustion fronts). This approach gives us the solution of the macro model (1) via the limit (8). The micro model (9) is only solved explicitly in a small region around a nonclassical wave in (1) while in the remaining domain any standard solver can be used on a macroscale grid. Using the numerical fluxes developed in [3] we construct a solver that is conservative on the macroscale. Let us emphasize that we are *not* interested in the complete solution of the microscale model rather in the correct behaviour of the solution on the macroscale.

This work is restricted to scalar equations. We expect that it can be extended to systems' cases. The main challenge will be to obtain a-priori knowledge on the exact Riemann solution for the microscale problem, which allows a validated estimate on the speed of the undercompressive wave which is then just one of several waves.

Let us give a short outline on the rest of the paper. After the short discussion of specific regularized models in Sect. 2, in Sect. 3 we present the concept of the new HMM-algorithm. In Sect. 4 we test the HMM-algorithm on Riemann problems for the examples from Sect. 2. In Sect. 5 we validate the HMM-algorithm and test it for a more general initial condition in Sect. 6.

2. **Model problems with nonclassical waves.** In this section we recall three microscale models which can be written in the form (9). Two of them provide toy problems in the theory of phase transition dynamics, one describes two-phase flow in porous media with rate-dependent capillary pressure.

2.1. **Local diffusive-dispersive regularization.** Compressible flow with liquid-vapour transitions can be governed by the Navier-Stokes-Korteweg equations [2], which contain second-order operators to model viscosity effects as well as third-order terms for the effects of capillary forces close to phase boundaries. A standard toy problem is given with the concave-convex flux $f(U) = U^3$ in (1), state space $\mathcal{U} = \mathbb{R}$ and the diffusive-dispersive operator

$$R^\varepsilon[\lambda; u] := \varepsilon u_{xx} + \lambda\varepsilon^2 u_{xxx}, \qquad \lambda \in (0, \infty) \tag{10}$$

in the microscale ansatz (9). For this model it has been proven in [9] that it allows for traveling wave solutions connecting states U^- and U^+ such that (3) is undercompressive. Furthermore it is known that a subsequence of solutions $u^{\varepsilon,\lambda}$ converges to a weak solution U^λ of (1) for $\varepsilon \to 0$. It is important to note that the limit depends on the parameter λ. This is also visible for the following special weak solution for Riemann initial data that can be realized as the limit in (8) (cf. [13])

$$U^\lambda(x,t) = \begin{cases} U^l & \text{for } x \le s_1 t, \\ u^m := -U^l + \frac{1}{3}\sqrt{\frac{2}{\lambda}} & \text{for } s_1 t < x \le s_2 t, \\ U^r & \text{for } s_2 t < x. \end{cases} \qquad (U^l > 0 > U^r > u^m) \tag{11}$$

The shock speeds are given by $s_1 = s(U^l, u^m)$, $s_2 = s(u^m, U^r)$ with the notation from (4). Note that U^r has to be sufficiently close to u^m, for details see [13]. We will use (11) as reference solution in Sect. 5. An approximation $u^{\varepsilon,\lambda}$ of the solution U^λ with the slow undercompressive shock wave is displayed in Fig. 3 (left viewgraph).

2.2. **Nonlocal diffusive-dispersive regularization.** In the theory of phase transitions in compressible media local differential operators as in (10) can be viewed as an approximation to more general nonlocal operators [18]. We consider as an instance the macroscale model (1) as in Sect. 2.1 but for the microscale model (9) a nonlocal regularization given through

$$R^\varepsilon[\lambda; u] := \varepsilon u_{xx} + \lambda\left[\int_{-\infty}^{\infty} \phi_\varepsilon(x-y)(u(y)-u(x))\,dy\right]_x, \qquad \lambda \in (0, \infty). \tag{12}$$

Here we have $\phi_\varepsilon(x) := \frac{1}{\varepsilon}\phi\left(\frac{x}{\varepsilon}\right)$ where ϕ is a nonnegative function which we will always choose as

$$\phi(x) := \exp\left(\frac{1}{x^2-1}\right) \Big/ \int_{-1}^{1} \exp\left(\frac{1}{y^2-1}\right) dy \quad \text{for} \quad x \in (-1,1), \tag{13}$$

and equal to 0 elsewhere. For (12) analogous results as for the local choice are known [17, 15]. We refer to Fig. 5, left viewgraph, for a typical solution with slow undercompressive wave and fast rarefaction wave. However, it is not known whether

the weak solution U^λ generated by (8) with operator (12) can also be characterized by a kinetic relation as in (7).

2.3. **Two-phase flow process with rate-dependent capillary pressure.** In this part we consider two-phase flow in porous media. In the macroscale model (1) we choose the convex-concave Buckley-Leverett flux

$$f(U) = \frac{U^2}{U^2 + M(1-U)^2} \quad \text{for} \quad U \in \mathcal{U} := [0,1], \tag{14}$$

where U stands for the unknown water saturation and $M > 1$ describes the oil/water viscosity ratio. For the regularization we use

$$R^\varepsilon[\lambda; u] := \varepsilon u_{xx} + \lambda \varepsilon^2 u_{xxt} \qquad (\lambda \in (0, \infty)). \tag{15}$$

This type of rate-dependent regularization has been suggested in [12]. It extends the static capillary pressure approach to model dynamic effects in the pressure difference between the two phases.

For the regularized problem (9) with (15) it is again known that traveling wave solutions exist as profiles for undercompressive shock waves in the limit $\varepsilon \to 0$ [6]. A typical solution for Riemann initial data with slow Laxian wave and fast undercompressive wave is illustrated in Fig. 8 (left viewgraph). An explicit kinetic relation as in (7) is not known up to our knowledge.

3. **Computation of nonclassical waves with a heterogeneous multiscale method.** Before we present our numerical approach let us note that a solution which contains nonclassical waves cannot be approximated by a standard scheme as e.g. a monotone Finite Volume method. These are constructed to converge to the Kruzkov solution excluding such waves. Therefore special methods as in [5, 3] have been constructed. However these methods rely on an explicitly given kinetic relation while our approach utilizes the regularized model.

3.1. **The heterogeneous multiscale algorithm.** We determine the macroscale approximation for (1) and the microscale approximation for (9) on a coarse and a fine space-time grid, respectively.

We denote symbols of the macroscale model by capital letters and the ones of the microscale model with lower case letters.

We use constant grid parameters $\Delta X > 0$ and $\Delta x > 0$ for the space discretization both on the macroscale and on the microscale. Furthermore we set $X_j = j\Delta X$, $j \in \mathbb{Z}$. The approximation of the macroscale solution at discrete times $0 =: T^0 < T^1 < T^2 < \dots$ is a function constant on each cell $\mathcal{C}_j = [X_{j-1/2}, X_{j+1/2})$. For the initialization of the Finite Volume type scheme on the macroscale we define the sequence $\left(U_j^0\right)_{j\in\mathbb{Z}}$ of averaged values by

$$U_j^0 = \frac{1}{\Delta X} \int_{\mathcal{C}_j} U_0(x)\, dx.$$

Furthermore we collect all cell boundaries $X_{j+1/2}$, say $\Gamma \in \mathbb{N}$, such that $f''(U_j^0)$ and $f''(U_{j+1}^0)$ have different sign in the set $(X_\gamma^0)_{\gamma=1,\dots,\Gamma}$ of discrete front positions.

Algorithm 1 below determines for all times T^n the macroscale approximation $U^n := (U_i^n)_{i\in\mathbb{Z}}$ and the approximate front positions $(X_\gamma^n)_{\gamma=1,\dots,\Gamma}$ for nonclassical shock waves. The space-time domain for which the microscale problem has to be solved is defined by $\mathcal{D}_\gamma^n := (x_\gamma^{n,l}, x_\gamma^{n,r}) \times (T^n, T^n + t_\gamma^n)$ with $x_\gamma^{n,l} < X_\gamma^n < x_\gamma^{n,r}$ and $t_\gamma^n > 0$. We now give the main HMM-algorithm in a rather general manner. The

algorithm will be commented and detailed below. For the sake of simplicity we restrict ourselves to monotone increasing flux functions with at most one inflection point $\bar{U}$ with $f'''(\bar{U}) > 0$.

Algorithm 1. Input: $n = 0$, ε, λ, $(U_j^0)_{j\in\mathbb{Z}}$, $(X_\gamma^0)_{\gamma=1,\dots,\Gamma}$, $(X_j)_{j\in\mathbb{Z}}$, $\mathcal{D}_\gamma^0$
DO
{

1. **The reconstruction.** We reconstruct according to the location of the discrete front X_γ^n, $\gamma = 1,\dots,\Gamma$,
$$u_\gamma(x, T^n) := \begin{cases} U_{s-1}^n =: u_\gamma^- & \text{for } X_\gamma^n \le x, x \in \mathcal{D}_\gamma^n, \\ U_{s+1}^n =: u_\gamma^+ & \text{for } x < X_\gamma^n, x \in \mathcal{D}_\gamma^n, \end{cases}$$
with $X_\gamma^n \in [X_{s-1/2}, X_{s+1/2})$.
2. **Solving the microscale model.** For $\gamma = 1,\dots,\Gamma$ we solve (9) on $\mathcal{D}_\gamma^n$ with the initial data $u_\gamma(., T^n)$ and denote the solution by $u_\gamma : \mathcal{D}_\gamma^n \to \mathcal{U}$.
3. **Approximate middle state/data analysis.** For $\gamma = 1,\dots,\Gamma$ we determine a middle state u_γ^m between the two (approximate) shock waves in the solution u_γ of the microscale model.
4. **Computing the approximate front velocities.** For $\gamma = 1,\dots,\Gamma$ we compute the approximate velocity v_γ^n of the fronts by
$$v_\gamma^n = (f(u_\gamma^-) - f(u_\gamma^m))/(u_\gamma^- - u_\gamma^m).$$
5. **Computing the macroscale time step ΔT^n.** We compute the macroscale time step ΔT^n such that
$$\sup_{j\in\mathbb{Z}} \frac{\Delta T^n |f'(U_j^n)|}{\Delta X} < 1 \quad \text{and} \quad \max_{\gamma=1,\dots,\Gamma} \frac{\Delta T^n |f'(u_\gamma^m)|}{\Delta X} < 1,$$
and set $T^{n+1} = T^n + \Delta T^n$.
6. **Moving the fronts.** With the front velocities from step 4 we obtain the new location of the fronts by
$$X_\gamma^{n+1} = X_\gamma^n + v_\gamma^n \Delta T^n, \quad \gamma = 1,\dots,\Gamma.$$
7. **Updating the macroscale variable U^n.** We get the new macroscale variables $(U_j^{n+1})_{j\in\mathbb{Z}}$ by evolving (1) with a Finite Volume scheme
$$U_j^{n+1} = U_j^n - \frac{\Delta T^n}{\Delta X}\left(f_{j+\frac{1}{2}}^n - f_{j-\frac{1}{2}}^n\right), \quad j \in \mathbb{Z}, \tag{16}$$
where $f_{j+\frac{1}{2}}^n$ is a special numerical flux function (see (17) below).
8. $n \to n+1$

}
UNTIL $T^n \ge T$.

It is necessary to make more precise some of the steps in Algorithm 1 but let us make several notes in advance.

Remark 1. (i) The scaling parameter $\varepsilon > 0$ in Algorithm 1 has the role of a discretization parameter: the smaller we choose it the more accurate is the prediction of the front velocities and thus the error of the macroscale approximation. Ideally this error is in the same range as the error induced by the grid parameter ΔX. We show the effect of the choice of ε in Sect. 5.1.

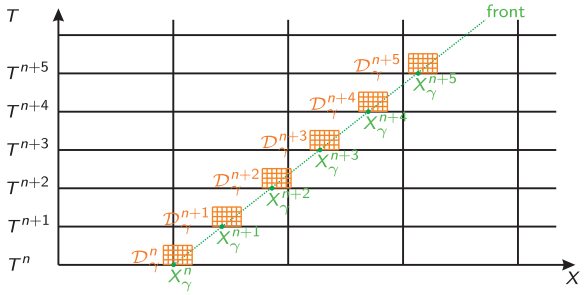

FIGURE 1. Macroscale computational domain Ω_T and microscale computational domain $\mathcal{D}_\gamma^n$ for a propagating front γ intersecting the macroscale time levels T^n in X_γ^n.

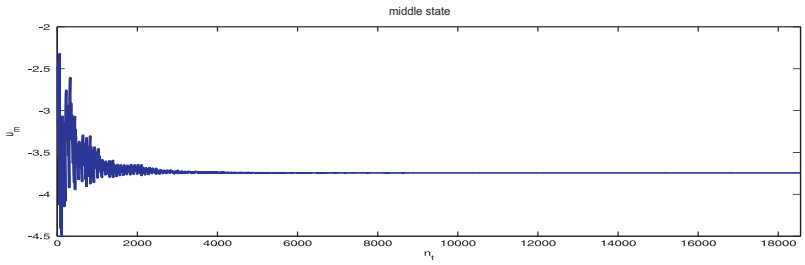

FIGURE 2. Approximate middle state u_γ^m versus microscale time steps for a whole macroscale time step ΔT^n.

(ii) In the reconstruction (step 1) we use for the states u_γ^- and u_γ^+ the values U_{s-1}^n and U_{s+1}^n respectively (instead of the apparently more natural value U_s^n for one of the two states). This enables us to use a numerical flux (cf. (17) below) in step 7 which guarantees mass conservation (for a detailed explanation see discussion at the end of the section).

(iii) We have not said how to solve numerically the micro model in step 2. This depends in fact on the micro model under study. In Sect. 4 we present some adequate numerical schemes. Let us note that there are completely different possibilities as the numerical use of the Dafermos regularization [1].

(iv) The computational success of Algorithm 1 hinges on the size of the microscale domains $\mathcal{D}_\gamma^n$. In particular the microscale time t_γ^n has to be small to limit the expensive microscale computations. We illustrate this in Fig. 1. On the other hand we have to determine the middle state u_γ^m from the computation. This is done by some data analysis which gives more stable results with an increasing number of microscale time steps. This is visualized in Fig. 2, where the middle state u_γ^m is computed over a whole macroscale time step ΔT^n.

For simplicity we have used in our computations for $n \in \mathbb{N}$ the same size of the microscale domain $\mathcal{D}_\gamma^n$, placed at the corresponding front position X_γ^n. In Sect. 4.1 - 4.3 the respective sizes of the domain $\mathcal{D}_\gamma^n$ are stated. There one can see well that the size of the microscale domain depends strong from the considered problem and make use of experienced data. In general the domain has to be at least as big as a constant middle state can be build out.

(v) In Algorithm 1 we have supposed implicitly that the number of fronts remains constant, equal to Γ. If two nonclassical shocks join to one Algorithm 1 has to be modified in a straightforward way.

(vi) In case the kinetic function is known the HMM do not have an advantage over the algorithm proposed in [3]. The computational overhead is exactly the time needed for solving the microscale model in step 2 and computing the middle state u_γ^m in step 3 which corresponds the kinetic relation. On the other hand the algorithm proposed in [3] cannot be used for problems with unknown kinetic function, this is exactly one of the motivations of the HMM.

In Step 3 of Algorithm 1 we determine the middle state u_γ^m through some data analysis. What is meant is that the results of the microscale computation at time $T^n + t_\gamma^n$ are scanned: the value with the smallest absolute discrete slope (and not close to $u_\gamma^\pm$) is chosen as u_γ^m. This step requires definitely some a-priori knowledge of the exact microscale solution.

It remains to define the numerical fluxes in step 7. Here we follow the construction in [3], precisely

$$\Delta T^n f_{j+\frac{1}{2}}^n = \tag{17}$$
$$\begin{cases} \min\left(\Delta T_{j+\frac{1}{2}}, \Delta T^n\right) f(U_{j,r}^n) + \max\left(\Delta T^n - \Delta T_{j+\frac{1}{2}}, 0\right) f(U_{j,l}^n), & d_j^n \in [0,1], \\ \Delta T^n f(U_j^n), & \text{else}, \end{cases}$$

with

$$\Delta T_{j+1/2} = \frac{1-d_j^n}{s(U_{j,l}^n, U_{j,r}^n)} \Delta X, \qquad U_{j,l}^n = U_{j-1}^n, \quad U_{j,r}^n = u_\gamma^m. \tag{18}$$

We used $d_j^n = (U_{j,r}^n - U_j^n)/(U_{j,r}^n - U_{j,l}^n)$ and $s(U_{j,l}^n, U_{j,r}^n)$ is given in (4).
This flux function has been introduced in [3] to compute solutions of (1) with nonclassical waves that satisfy a kinetic relation like in (7). However in the original flux the kinetic relation is just used to compute the middle states like our value u_γ^m. Due to this observation we can also make use of the approach and can benefit from its advantages: the Finite Volume like scheme in step 7 conserves mass, i.e. (cf. Property 2 in [3]):

$$\sum_{j\in\mathbb{Z}} U_j^n = \sum_{j\in\mathbb{Z}} U_j^0 \qquad \forall\, n \in \mathbb{N}_0.$$

Another important feature of the scheme is that by construction the nonclassical wave is only smeared out on three cells with exactly one cell average in this discrete layer (see also Remark 1(ii) on the choice of the reconstruction).

4. Heterogeneous multiscale algorithm for model problems with nonclassical waves.

In this part we use Algorihm 1 from Sect. 3 for the model problems introduced in Sect. 2. For every example we give first the discretization of the microscale model, and then present some numerical examples.

For the sake of simplicity we use Finite Difference methods for the microscale problem. Let us stress that the heterogeneous approach can be improved considerably if more efficient schemes are used for the computation of the smooth solution of the microscale problem, as e.g. high-order Discontinuous Galerkin methods (cf. [11] for the application of this method on the model problems for phase transition).

4.1. **Local diffusive-dispersive regularization.** For the discretization of (9) with (10) we use a fourth-order discretization for the flux function suggested by Hayes and LeFloch [10]. The complete scheme has then the form

$$u_i^{n+1} = u_i^n - \frac{\Delta t}{\Delta x}\left(g_{i+1/2} - g_{i-1/2}\right) + \varepsilon\frac{\Delta t}{\Delta x^2}\left(u_{i+1}^n - 2u_i^n + u_{i-1}^n\right) + \lambda\varepsilon^2\frac{\Delta t}{2\Delta x^3}\left(u_{i+2}^n - 2u_{i+1}^n + 2u_{i-1}^n - u_{i-2}^n\right)$$

with the fourth-order flux

$$g_{i+1/2} = \frac{1}{12}\left(-(u_{i+2}^n)^3 + 7(u_{i+1}^n)^3 + 7(u_i^n)^3 - (u_{i-1}^n)^3\right).$$

In Fig. 3 we consider results of Algorithm 1 with the initial datum

$$U_0(x) = U^l = 4,0 \text{ for } x < 0 \quad \text{and} \quad U_0(x) = U^r = -2,5 \text{ for } x > 0, \tag{19}$$

discretization data

$$\varepsilon = 10^{-5},\ \lambda = 4,\ \Delta x = 4\cdot 10^{-6},\ \Delta X = 0,01\,, \tag{20}$$

and a space-time domain $\mathcal{D}_\gamma^n$ with $|x_\gamma^{n,r} - x_\gamma^{n,l}| = 200\Delta x$, $t_\gamma^n = 7000\Delta t$.
The exact limit solution is given by (11). The second and third viewgraph show for two different times the propagation of a nonclassical and a fast classical shock wave. As (constant) time step on the macroscale we get $\Delta T = 2,0\cdot 10^{-4}$. In the first viewgraph we present a result of a separate computation for the microscale model with the same data. One observes that due to the upscaling process in Algorithm 1 details of the microscale solution as the oscillations around the Laxian wave are suppressed. Note that this calculation leads to the microscale time step $\Delta t = 3,2\cdot 10^{-9}$.

In Fig. 4 we show analogous results with the same data as in (19), (20) but for the initial condition

$$U_0(x) = 4,0 \text{ for } x < 0 \quad \text{and} \quad U_0(x) = -5,0 \text{ for } x > 0,$$

and $|x_\gamma^{n,r} - x_\gamma^{n,l}| = 300\Delta x$, $t_\gamma^n = 7000\Delta t$ for the domain $\mathcal{D}_\gamma^n$.
The solution consists now of a nonclassical shock wave and a rarefaction wave.

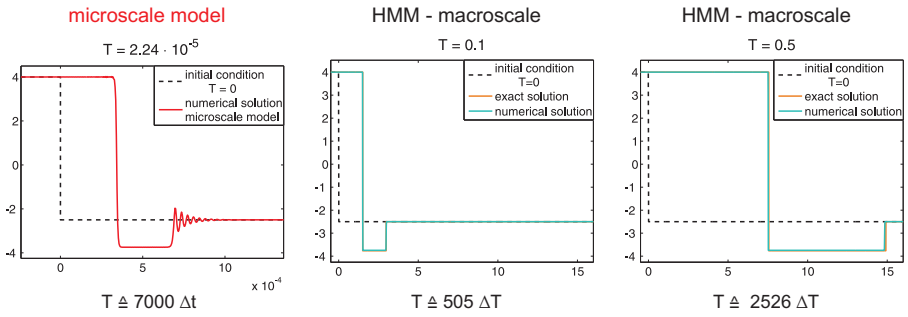

FIGURE 3. Shock-shock solution for local regularization (10).

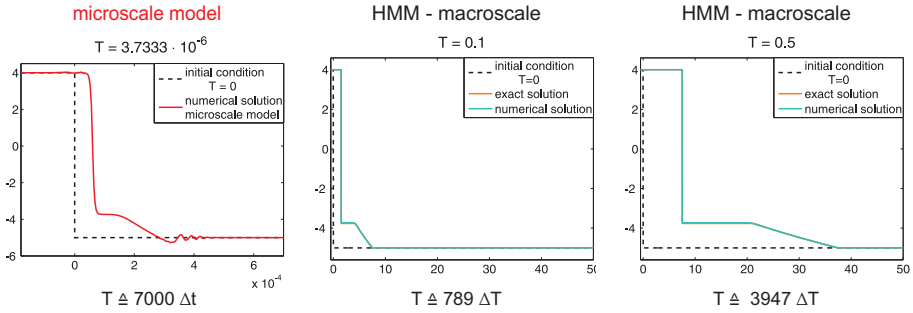

FIGURE 4. Shock-rarefaction solution for local regularization (10).

4.2. **Nonlocal diffusive-dispersive regularization.** For the microscale model (9), (12) with $f(U) = U^3$ we use upwinding for the fluxes and discretize the integral with a one-point rule in the cell boundaries. This results in the scheme

$$u_i^{n+1} = u_i^n - \frac{\Delta t}{\Delta x}\left(f(u_i^n) - f(u_{i-1}^n)\right) + \varepsilon\frac{\Delta t}{(\Delta x)^2}\left(u_{i+1}^n - 2u_i^n + u_{i-1}^n\right)$$
$$+ \lambda\Delta t \sum_{k=-m}^{m} u_{i+k}^n\, G_k^\varepsilon - \lambda\frac{\Delta t}{\Delta x}\left(u_i^n - u_{i-1}^n\right),$$

with the weights $G_j^\varepsilon = \phi_\varepsilon\left(x_{j+\frac{1}{2}}\right) - \phi_\varepsilon\left(x_{j-\frac{1}{2}}\right)$ (cf. (13)) [14]. One can check that this choice implies that the scheme is in particular conservative.

In the same format as in Sect. 4.1 we display numerical results in Fig. 5 for initial datum

$$U_0(x) = 4,0 \text{ for } x < 0 \quad \text{and} \quad U_0(x) = -2,0 \text{ for } x > 0, \tag{21}$$

discretization data

$$\varepsilon = 10^{-4},\ \lambda = 15,\ \Delta x = 5,7 \cdot 10^{-6},\ \Delta X = 0,01\,, \tag{22}$$

and $|x_\gamma^{n,r} - x_\gamma^{n,l}| = 600\Delta x$, $t_\gamma^n = 2000\Delta t$.
For Fig. 6 the same parameters are used but for initial datum

$$U_0(x) = 4,0 \text{ for } x < 0 \quad \text{and} \quad U_0(x) = -5,0 \text{ for } x > 0, \tag{23}$$

and $|x_\gamma^{n,r} - x_\gamma^{n,l}| = 1500\Delta x$, $t_\gamma^n = 2000\Delta t$.

For the nonlocal case no exact limit solutions like (11) are known but we observe qualitatively the same effects. In Fig. 7 the dependence of the estimated state u_γ^m on the microscale parameter ϵ is visualized for different parameters λ.

4.3. **Two-phase flow process with rate-dependent capillary pressure.** To discretize the microscale model (9) with regularization (15) we rewrite it in the form

$$w = u_t, \qquad \left(I - \varepsilon^2\lambda\frac{d^2}{dx^2}\right) w = \varepsilon u_{xx} + f(u)_x. \tag{24}$$

A straightforward Finite Difference discretization of the second equation in (24) leads at each microscale time level to a linear system for the w_i^n's. For a uniform grid the system matrix is a tridiagonal matrix for which the inverse can be determined with the so-called HMGTI algorithm from [8]. We use this algorithm and update the u_i^n's by an explicit Euler step for the first equation in (24). Note that the flux from (14) is convex-concave, we have $f'''(\bar{U}) < 0$ in the unique inflection point

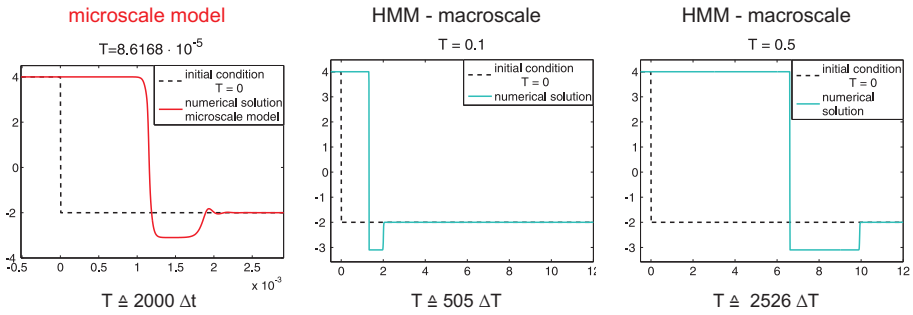

FIGURE 5. Shock-shock solution for nonlocal regularization (12).

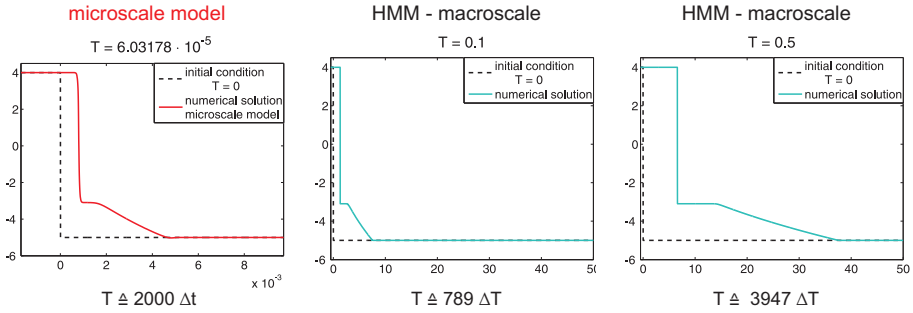

FIGURE 6. Shock-rarefaction solution for nonlocal regularization (12).

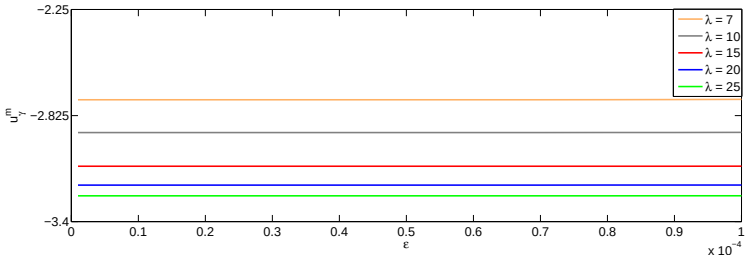

FIGURE 7. Dependence of the estimated state u_γ^m on the microscale parameter ϵ.

$\bar{U} \in (0,1)$. Therefore we have to exchange u_γ^- with u_γ^+ in Step 4 of Algorithm 1. In addition we have to use $U_{j,l}^n = u_\gamma^m$ and $U_{j,r}^n = U_{j+1}^n$ in (18) for the computation of the numerical flux in step 7 of Algorithm 1.

In Figs. 8 and 9 we consider in the format as in Sect. 4.1 results of Algorithm 1 with the initial data

$$\begin{aligned} U_0(x) &= 0,8 \text{ for } x < 0 \quad \text{and} \quad U_0(x) = 0 \text{ for } x > 0 \text{ (Fig. 8)}, \\ U_0(x) &= 1,0 \text{ for } x < 0 \quad \text{and} \quad U_0(x) = 0 \text{ for } x > 0 \text{ (Fig. 9)}, \end{aligned} \tag{25}$$

and discretization data

$$\varepsilon = 10^{-5},\ \lambda = 5,\ M = 2,\ \Delta x = 1,5 \cdot 10^{-5},\ \Delta X = 0,02.$$

The parameters for the domain $\mathcal{D}_\gamma^n$ are $|x_\gamma^{n,r} - x_\gamma^{n,l}| = 450\Delta x$, $t_\gamma^n = 700\Delta t$ (Fig. 8) and $|x_\gamma^{n,r} - x_\gamma^{n,l}| = 300\Delta x$, $t_\gamma^n = 400\Delta t$ (Fig. 9) respectively.

We now see that the nonclassical wave acts as the (fast) precursor front for the invading water phase. It is interesting to see that in the microscale computation in the mostleft viewgraph of Fig. 8 the data do not oscillate and do not take values outside $\mathcal{U} = [0, 1]$. Compare the result with the corresponding plots in Figs. 3, 5.

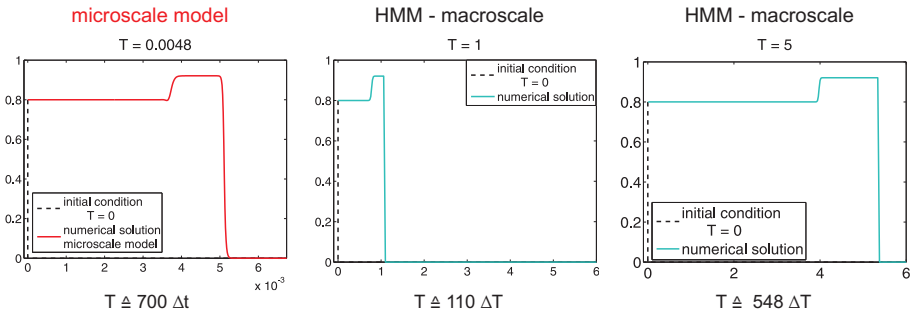

FIGURE 8. Invading water front with overshoot for regularization (15).

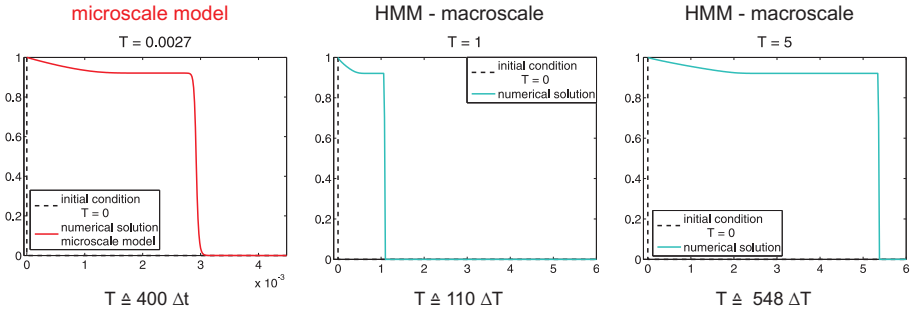

FIGURE 9. Invading water front with trailing wave for regularization (15).

5. **Performance of the heterogeneous multiscale method.** In this section we examine Algorithm 1 on aspects of convergence, mass conservation, and computational complexity.

We use the regularized problem (10) with the cubic flux $f(U) = U^3$ together with the initial datum from (19) as the test problem to validate our approach. In this case we can use (11) as the exact solution of the macroscale problem in the sense of the limit in (8).

5.1. **Convergence and conservation of mass.** We compute the solution for (1) with the regularization (10) with different macroscale grid sizes $\Delta X \in \{0.5, \ldots, 0.01\}$. The solutions are depicted in Fig. 10 with appropriate zooms into the shock waves. One can see well that for smaller macroscale grid size ΔX the shock waves are better resolved and we can observe convergence of the scheme.

In Fig. 11 (left) the error between the numerical solution for different macroscale grid sizes and the limit solution (11) is plotted in the L^1-norm. We observe that the L^1-error decreases followed by a saturation effect. This means that it doesn't make sense anymore to refine the macroscale grid from $\Delta X = 0.1$ because the error in the L^1-norm is dominated by the error which arises by the calculation of the value u_γ^m at the microscale, see Remark 1(i), and we should instead scale down the parameter ε. The slight increase of the error in Fig. 11 (left) is caused by the value lying in the layer of the nonclassical shock on the macroscale.

Furthermore we have checked the conservation of mass of the scheme for the update on the macroscale of step 7 in Algorithm 1. The result confirms what we know from the construction of the numerical flux in (17), see Fig. 11 (right).

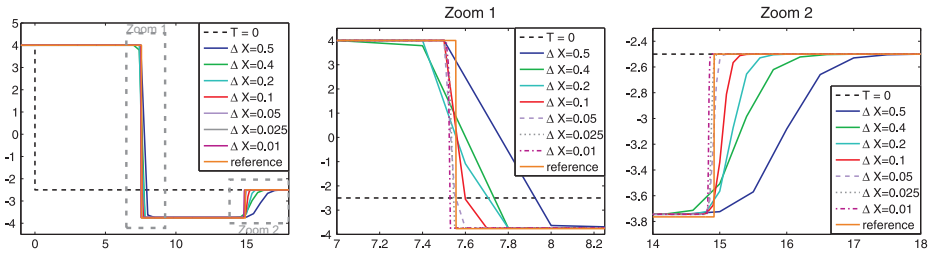

FIGURE 10. Macroscale approximation with $\varepsilon = 10^{-5}$, $\lambda = 4$, zooms into the shock waves for different grid sizes.

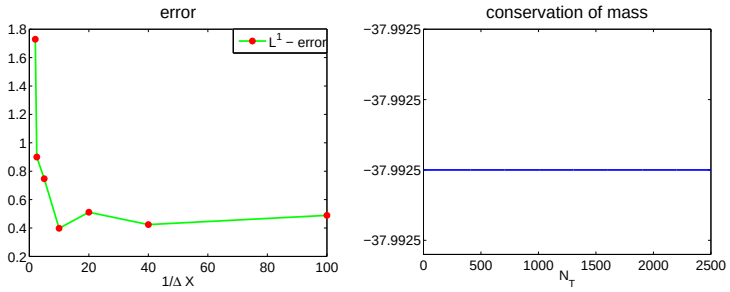

FIGURE 11. Error in L^1-norm (left) and mass conservation (right).

5.2. **Computational complexity for the heterogeneous multiscale approach.** As long as an explicit kinetic relation as in (7) is not known the limit solution U^λ from (8) can only be approximated by solving the microscale model (9) on the complete macroscale computational domain with some scheme (direct approach). Algorithm 1 using the same scheme on the microscale should be at least more efficient than the direct approach. In Table 1 we present a comparison of cpu-times which underlines the efficiency of Algorithm 1. For the grid sizes of the computation we use the same values as in Sect. 4.1. Note that the cpu-times for the microscale model on the macroscale domain are estimated values. They have been extrapolated from computations on a smaller space-time domain.

One could argue that the use of an adaptive solver for the microscale computation could lead to a worse performance of Algorithm 1. But note that we can also use

this solver within the Heterogeneous Multiscale Method. Moreover it has to be stressed that the time length of the microscale domain $\mathcal{D}_\gamma^n$ is much smaller than the macroscale time step. This can not be achieved for the direct approach.

T	macroscopic model		microscopic model	
	N_T	cpu-time	n_t	cpu-time
$1,98 \cdot 10^{-4}$	1	7,52 sec.	$6,19 \cdot 10^4$	$9,2 \cdot 10^5$ sec. ≈ 11 days
0,1	505	20,41 sec.	$3,13 \cdot 10^7$	$4,6 \cdot 10^8$ sec. ≈ 15 years
0,5	2526	22,76 sec.	$1,56 \cdot 10^8$	$2,3 \cdot 10^9$ sec. ≈ 73 years
	$N_X = 1650$, $n_x = 400$		$n_x = 4125000$	

TABLE 1. Cpu-time for Algorithm 1 versus cpu-time for direct approach. N_T (n_T) stands for the number of macroscale (microscale) time steps, N_x (n_x) for the number of macroscale (microscale) cells.

6. **Heterogeneous multiscale method for Non-Riemann initial data.** Up to now we only have considered Riemann problems. This was helpful since we knew the exact solution in some cases and could validate Algorithm 1. Finally we consider a problem for (10) with more general initial data, namely

$$U_0(x) = 4\sin(2\pi x) \text{ for } x \in (0,1) \quad \text{and} \quad U_0 \equiv 0 \text{ elsewhere.} \tag{26}$$

All other parameters are as in Sect. 4.1.

We can observe from Fig. 12 that the approximation firstly rears up and forms a front from the continuous initial function. After this the solution develops a nonclassical shock wave, forms a nonclassical shock-rarefaction pattern, a classical shock and again a rarefaction and classical shock wave.

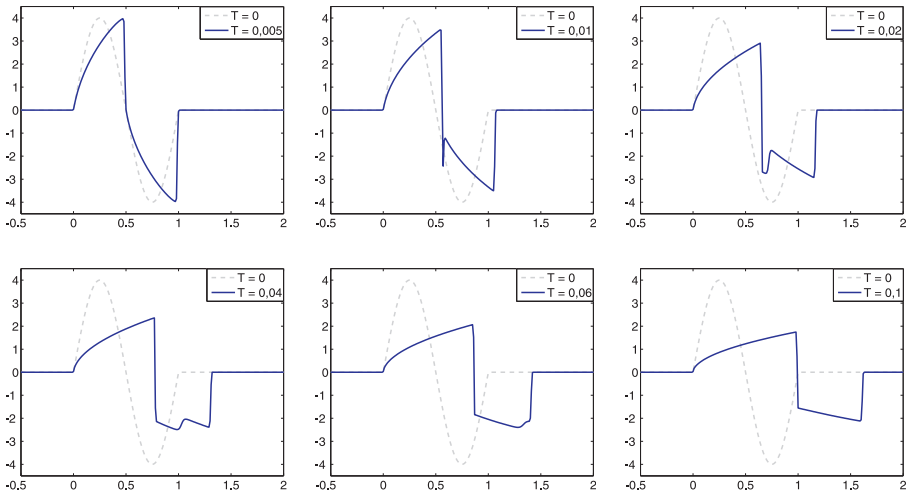

FIGURE 12. Solution of the Cauchy problem for (26) at different times.

REFERENCES

[1] A. Ambroso, B. Boutin, F. Coquel, E. Godlewski and P. G. LeFloch, "Coupling two Scalar Conservation Laws via Dafermos' Self-similar Regularization," K. Kunisch, G. Of and O.Steinbach (Eds), Proc. of ENUMATH 2007, Springer, 2008.

[2] D. M. Anderson, G. B. McFadden and A. A. Wheeler, *Diffuse-interface methods in fluid mechanics. Annual review of fluid mechanics*, Annu. Rev. Fluid Mech., Annual Reviews, Palo Alto, CA, **30** (1998), 139–165.

[3] B. Boutin, C. Chalons, F. Lagoutière and P. G. LeFloch, *Convergent and conservative schemes for nonclassical solutions based on kinetic relations*, Interfaces Free Bound., **10** (2008).

[4] N. Bedjaoui and P. G. LeFloch, *Diffusive-dispersive traveling waves and kinetic relations. I. Nonconvex hyperbolic conservation laws*, J. Differential Eq., **178** (2002), 574–607.

[5] C. Chalons and P. G. LeFloch, *Computing undercompressive waves with the random choice scheme. Nonclassical shock waves*, Interfaces Free Bound. 5, **2** (2003), 129–158.

[6] C. J. van Duijn, L. A. Peletier and I. S. Pop, *A new class of entropy solutions of the Buckley-Leverett equation*, SIAM J. Math. Anal., **39** (2007), 507–536.

[7] W. E. and B. Engquist, *The heterogeneous multiscale methods*, Comm. Math. Sci, **1** (2003), 87–132.

[8] M. El-Mikkawy and A. Karawia, *Inversion of general tridiagonal matrices*, Appl. Math. Lett., **19** (2006), 712–720.

[9] B. T. Hayes and P. G. LeFloch, *Nonclassical shocks and kinetic relations. Scalar conservation laws*, Arch. Rational Mech. Anal., **139** (1997), 1–56.

[10] B. T. Hayes and P. G. LeFloch, *Nonclassical shocks and kinetic relations: Finite difference schemes*, SIAM J. Numer. Anal., **35** (1998), 2169–2194.

[11] J. Haink and C. Rohde, *Local discontinuous-Galerkin schemes for model problems in phase transition theory*, Commun. Comput. Phys., **4** (2008), 860–893.

[12] S. M. Hassanizadeh and W. G. Gray, *Thermodynamic basis of capillary pressure in porous media*, Water Resour. Res., **29** (1993), 3389–3405.

[13] D. Jacobs, B. McKinney and M. Shearer, *Travelling wave solutions of the modified Korteweg-de Vries-Burgers equation*, J. Differential Eq., **116** (1995), 448–467.

[14] Frederike Kissling "Analysis und Numerik für ein Mehrskalenproblem in der Theorie der Phasenübergänge," Diploma thesis, Universität Stuttgart, 2009.

[15] F. Kissling, P. G. LeFloch and C. Rohde, *A kinetic decomposition for singular limits of non-local conservation laws*, J. Differential Eq. 247, **12** (2009), 3338–3356.

[16] P. G. LeFloch, "Hyperbolic Systems of Conservation Laws. The Theory of Classical and Nonclassical Shock Waves," Lectures in Mathematics ETH Zürich, Birkhäuser Verlag, Basel, 2002.

[17] C. Rohde, *Scalar conservation laws with mixed local and nonlocal diffusion-dispersion terms*, SIAM J. Math. Anal., **37** (2005), 103–129.

[18] C. Rohde, *On local and non-local Navier-Stokes-Korteweg systems for liquid-vapour phase transitions*, ZAMM Z. Angew. Math. Mech., **85** (2005), 839–857.

[19] Y. Sun and B. Engquist, *Heterogeneous multiscale methods for interface tracking of combustion fronts*, Multiscale Model. Simul., **5** (2006), 532–563.

Received January 2010; revised May 2010.

E-mail address: frederike.kissling@mathematik.uni-stuttgart.de
E-mail address: christian.rohde@mathematik.uni-stuttgart.de